

## Supporting Information:

# Theoretical Investigation of the Olefin Cycle in H-SSZ-13 for the Ethanol-to-Olefins Process using *ab initio* Calculations and Kinetic Models

Jonas Amsler,<sup>a</sup> Sarah Bernart,<sup>a</sup> Philipp N. Plessow,<sup>\*a</sup> and Felix Studt<sup>a,b</sup>

## Contents

<b>S1 EtOH dehydration barriers at 473.15 K and 573.15 K</b>	<b>1</b>
S1.1 Numerical treatment of adsorption kinetics . . . . .	2
<b>S2 Gas phase equilibrium of dehydration as a function of temperature</b>	<b>2</b>
<b>S3 Butene and hexene formation barriers with a common reference</b>	<b>3</b>
<b>S4 Reaction flow analysis</b>	<b>4</b>
<b>S5 vdW contribution in a parity diagram</b>	<b>5</b>
<b>S6 Location of bulkier transition states within the cavity</b>	<b>5</b>
<b>S7 Energy contributions</b>	<b>6</b>

## S1 EtOH dehydration barriers at 473.15 K and 573.15 K

In Table S1 we show the adsorption free energies and free energy barriers computed for the EtOH dehydration steps at 473.15 K and a reference pressure of 1 bar. The data for the same conditions, but a temperature of 573.15 K is presented in Table S2. Analogous to previous work, the reference concentration of the active site (ZOH) was set to  $17.9 \text{ mol m}^{-3}$ .<sup>1</sup>

**Table S1** Adsorption free energies of water, EtOH and DEE as well as forward and backward free energy barriers at 473.15 K and a reference pressure of 1 bar for all elementary reaction steps considered in the EtOH dehydration.

No.	Elementary reaction	$\Delta G^\ddagger \left( \frac{\text{kJ}}{\text{mol}} \right)$
1	$\text{ZOH} + \text{H}_2\text{O} \rightleftharpoons \text{ZOH}^*\text{H}_2\text{O}$	$-5^a$
2	$\text{ZOH} + \text{EtOH} \rightleftharpoons \text{ZOH}^*\text{EtOH}$	$-12^a$
3	$\text{ZOH} + \text{DEE} \rightleftharpoons \text{ZOH}^*\text{DEE}$	$-4^a$
4	$\text{ZOH}^*\text{EtOH} \rightleftharpoons \text{SES} + \text{H}_2\text{O}$	130, 118
5	$\text{SES} + \text{EtOH} \rightleftharpoons \text{ZOH}^*\text{DEE}$	110, 113
6	$\text{ZOH}^*\text{EtOH} + \text{EtOH} \rightleftharpoons \text{ZOH}^*\text{H}_2\text{O} + \text{DEE}$	146, 155
7	$\text{SES} \rightleftharpoons \text{ZOH} + \text{ethene}$	125, 147
8	$\text{ZOH}^*\text{EtOH} \rightleftharpoons \text{ZOH}^*\text{H}_2\text{O} + \text{ethene}$	176, 190
9	$\text{ZOH}^*\text{DEE} \rightleftharpoons \text{ZOH}^*\text{EtOH} + \text{ethene}$	171, 183

<sup>a</sup> adsorption free energies; low thermodynamically consistent barriers have been used for numerical reasons with no rate-limiting effect to the simulation results, see Section S1.1.

<sup>a</sup> Institute of Catalysis Research and Technology, Karlsruhe Institute of Technology, Hermann-von-Helmholtz-Platz 1, 76344 Eggenstein-Leopoldshafen, Germany. E-mail: plessow@kit.edu

<sup>b</sup> Institute for Chemical Technology and Polymer Chemistry, Karlsruhe Institute of Technology, Kaiserstr. 12, 76131 Karlsruhe, Germany.

**Table S2** Adsorption free energies of water, EtOH and DEE as well as forward and backward free energy barriers at 573.15 K and a reference pressure of 1 bar for all elementary reaction steps considered in the EtOH dehydration.

No.	Elementary reaction	$\Delta G^\ddagger$ ( $\frac{\text{kJ}}{\text{mol}}$ )
1	ZOH + H <sub>2</sub> O $\rightleftharpoons$ ZOH*H <sub>2</sub> O	10 <sup>a</sup>
2	ZOH + EtOH $\rightleftharpoons$ ZOH*EtOH	6 <sup>a</sup>
3	ZOH + DEE $\rightleftharpoons$ ZOH*DEE	16 <sup>a</sup>
4	ZOH*EtOH $\rightleftharpoons$ SES + H <sub>2</sub> O	130, 133
5	SES + EtOH $\rightleftharpoons$ ZOH*DEE	126, 129
6	ZOH*EtOH + EtOH $\rightleftharpoons$ ZOH*H <sub>2</sub> O + DEE	161, 172
7	SES $\rightleftharpoons$ ZOH + ethene	125, 163
8	ZOH*EtOH $\rightleftharpoons$ ZOH*H <sub>2</sub> O + ethene	176, 206
9	ZOH*DEE $\rightleftharpoons$ ZOH*EtOH + ethene	169, 199

<sup>a</sup> adsorption free energies; low thermodynamically consistent barriers have been used for numerical reasons with no rate-limiting effect to the simulation results, see Section S1.1.

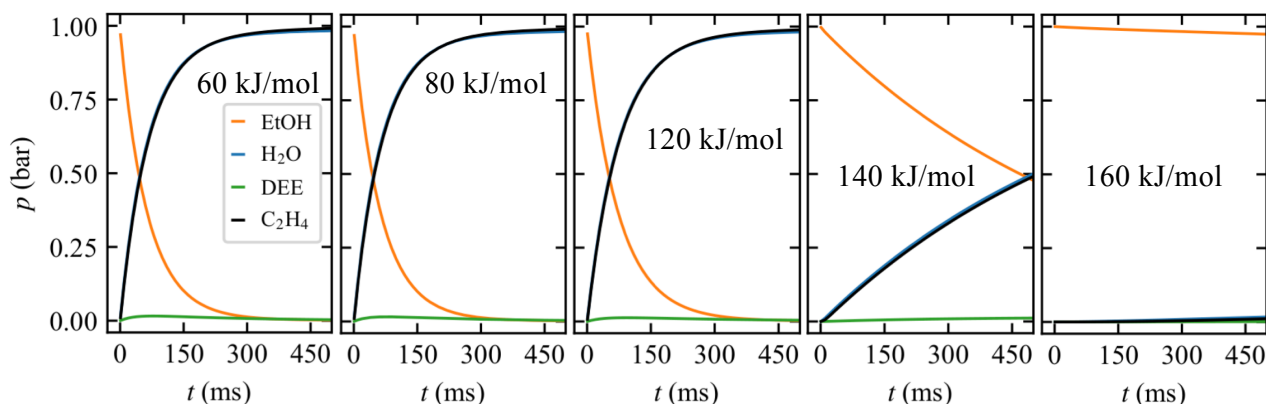


**Fig. S1** Simulated partial pressures of gas phase species using the reactions mechanism for EtOH dehydration from Figure 1 with varying numerical thresholds for the adsorption/desorption steps (60, 80, 120, 140, 160 kJ mol<sup>-1</sup>). Apart from the numerical thresholds all parameters are identical.

### S1.1 Numerical treatment of adsorption kinetics

We assume that adsorption steps are much faster than reaction steps such that adsorption equilibria are almost instantaneously equilibrated. Under this assumption, we use low thermodynamically consistent barriers for adsorption steps in the kinetic model. Here we choose 80 kJ mol<sup>-1</sup> as the numerical threshold which we assign to all adsorption/desorption barriers while the corresponding reversed process (desorption/adsorption) is assigned the same barrier shifted by the adsorption free energy for thermodynamic consistency. A higher numerical threshold allows us to choose larger time integration steps, hence faster simulations, but risks to influence the result if the threshold is too close to the reaction barriers. In Figure S1 we show that our chosen numerical threshold for adsorption/desorption steps has no influence on the simulation results. From the simulation with varying numerical thresholds we see that for 120 kJ mol<sup>-1</sup> and higher thresholds for adsorption/desorption steps, the results become biased by the threshold. For this reason we chose 80 kJ mol<sup>-1</sup> as the numerical threshold for adsorption/desorption steps.

## S2 Gas phase equilibrium of dehydration as a function of temperature

From the computed absolute free energies we can compute temperature-dependent equilibrium constants and thus the composition of the equilibrated gas phase as a function of the temperature. The equilibrium pressures based on an initial pressure of 1 bar EtOH are depicted in Figure S2 where only the gas phase species EtOH, DEE, H<sub>2</sub>O and C<sub>2</sub>H<sub>4</sub> were considered. Our computed equilibrium is in good agreement with experimental data by Garbarino *et al.* who measured the DEE:ethene ratio of 1:1 at roughly 370 K similar to our calculated value.<sup>2</sup> Likewise, they did not observe significant amounts of DEE at temperatures above 425 K.

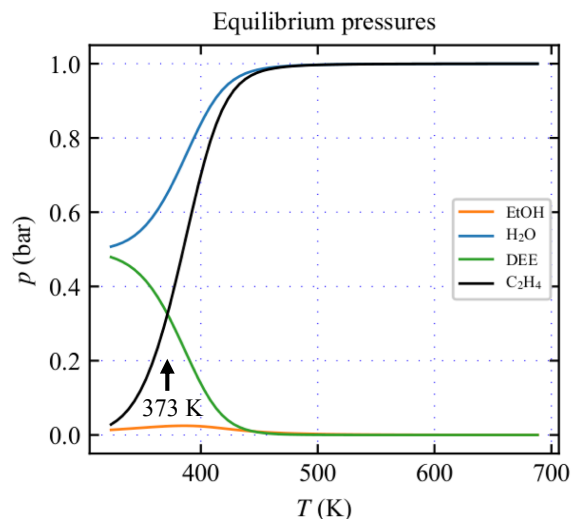


**Fig. S2** Computed gas phase composition after equilibration of 1 bar EtOH as a function of temperature. The considered gas phase species include EtOH, DEE, H<sub>2</sub>O and C<sub>2</sub>H<sub>4</sub>.

### S3 Butene and hexene formation barriers with a common reference

The barriers for butene and hexene formation in our article can be presented with a common reference, EtOH in the gas phase, that has also been used in Figure 1 and that corresponds to the starting conditions in our simulations. In Figure S3 we present the ethylation barriers of ethene from Figure 3 referenced to EtOH in the gas phase. We do not show the formation pathways to the ethylation agents

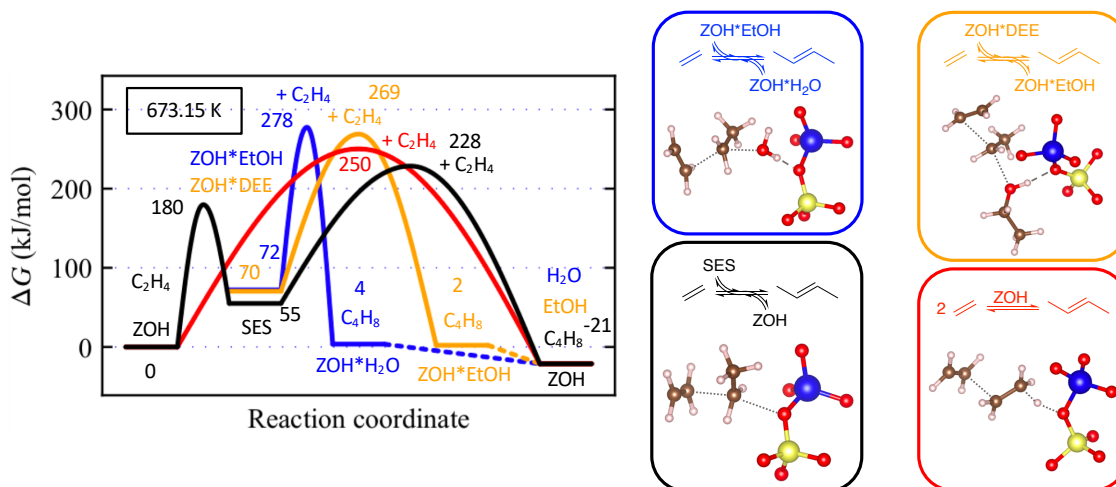


**Fig. S3** Gibbs free energy diagram and transition states for the ethylations of ethene at 673.15 K through EtOH directly (blue), DEE directly (orange), SES stepwise formed from ethene (black) and dimerization (red) at the acid site. All states are referenced to EtOH in the gas phase and then shifted so that the first shown state is at zero. The formation of the ethylation agents is shown in Figure 1.

– adsorbed EtOH (ZOH\*EtOH), adsorbed DEE (ZOH\*DEE), SES and ethene – in this Figure, because they are shown in Figure 1 and because ethene formation from EtOH is much faster than subsequent ethylation steps. The ethylation barriers of butene from Figure 4 referenced to EtOH in the gas phase are shown in Figure S4.

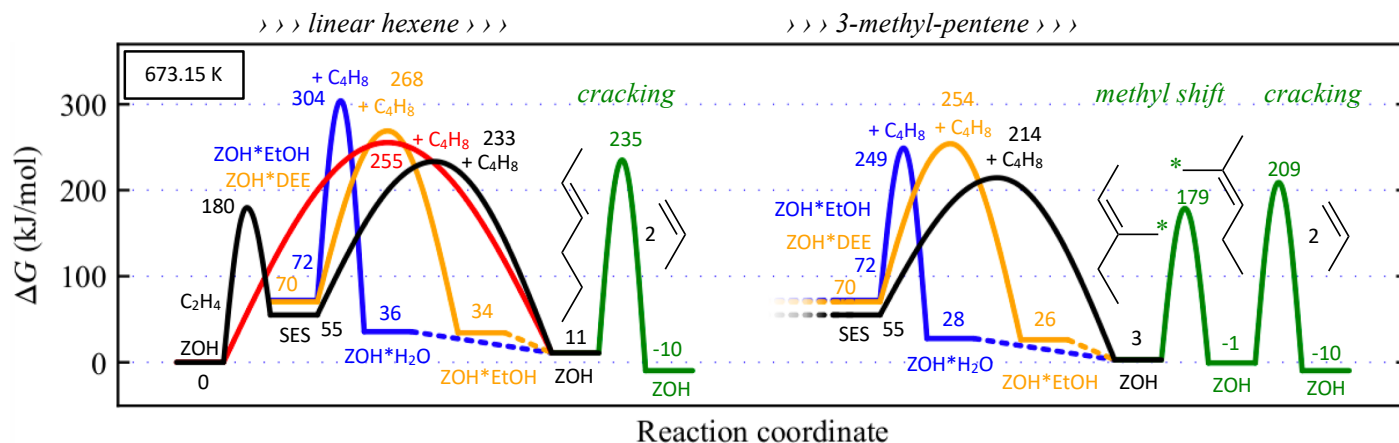


**Fig. S4** Gibbs free energy diagram for the ethylations of butene at 673.15 K through EtOH directly (blue), DEE directly (orange), SES stepwise formed from ethene (black) and dimerization (red) at the acid site. The formation and cracking of linear (left) and branched (right) hexene isomers can be compared. All states are referenced to EtOH in the gas phase and then shifted so that the first shown state is at zero. The formation of the ethylation agents is shown in Figure 1.

## S4 Reaction flow analysis

In this section we show the reaction flow analysis that was used to determine relevant reactions in EtOH dehydration and subsequent homologation and cracking steps. By tracking the cumulative throughput for each reaction path during the microkinetic simulation of our complete mechanism (reactions no. 1-23 in Tables 1-3) at 673.15 K, we obtained the data depicted in Figure S5. We observe that

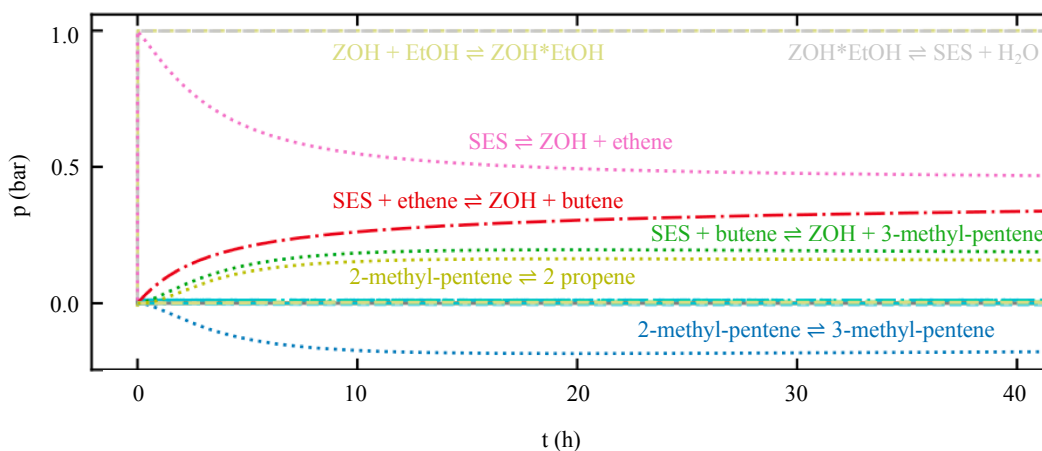


**Fig. S5** Reaction flows showing cumulative throughput of reaction paths for the complete mechanism at 673.15 K. The results for the most important reactions are labeled.

the stepwise dehydration pathway via reactions no. 2, 4 and 7 (indicated by arrows) is taken exclusively. Over the course of the process, however, about half of the formed ethene reacts back to SES, which is consumed in ethylations of ethene and butene. From this analysis of the reaction kinetics we see that the largest contributions come from reactions no. 2, 4, 7, 11, 17, 22 and 23.

## S5 vdW contribution in a parity diagram

The vdW part of the reaction barriers, here approximated with the D3 Grimme dispersion correction, largely depends on the size of the adsorbate.<sup>3</sup> For this reason we display the D3 contribution to the alkylation barriers in the parity plot in Figure S6. By comparing the parity plot in Figure 6 with the parity plot in Figure S6 we see that about 70 % of the differences in alkylation barrier height are caused by the D3 contribution ( $8 \text{ kJ mol}^{-1}$  shift in D3 contribution,  $11 \text{ kJ mol}^{-1}$  total shift). As expected the adsorbate size together with the confinement of the zeolite plays a significant role. However, the data points for linear and branched products do not group together in clusters as they do in for the total barriers in Figure 6. Hence, the preference for branched products does not come from the D3 contribution.

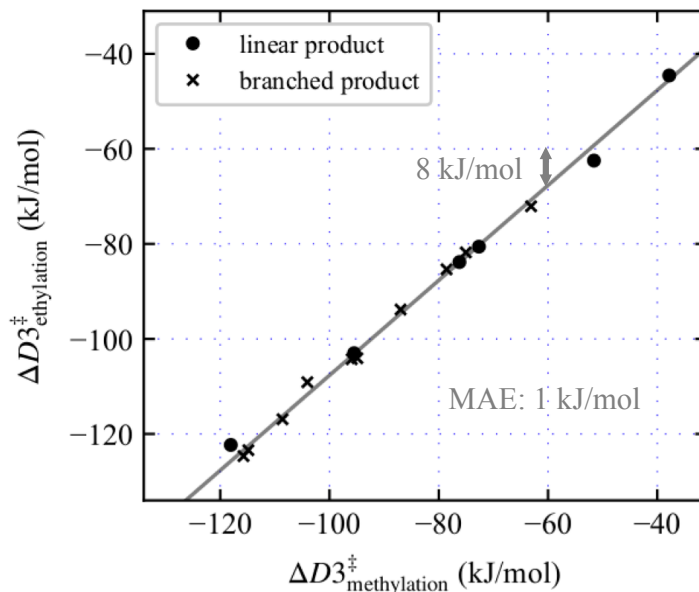


**Fig. S6** Correlation of D3 contributions to methylation and ethylation barriers, referenced to the gas phase, for the second step of the stepwise alkylation between ETO and MTO processes at 673.15 K and a reference pressure of 1 bar. The formation of linear and branched products is distinguished. The mean absolute error (MAE) is  $1 \text{ kJ mol}^{-1}$  from the diagonal with a slope of one and an offset of  $8 \text{ kJ mol}^{-1}$ .

## S6 Location of bulkier transition states within the cavity

Here, in Figure S7, we show the transition structure for the formation of 3-methyl-2-pentene via SES from different angles to visualize the orientation of the hydrocarbon chain inside the pore of the zeolite. The coordinates of all structures are attached as additional electronic supporting information.

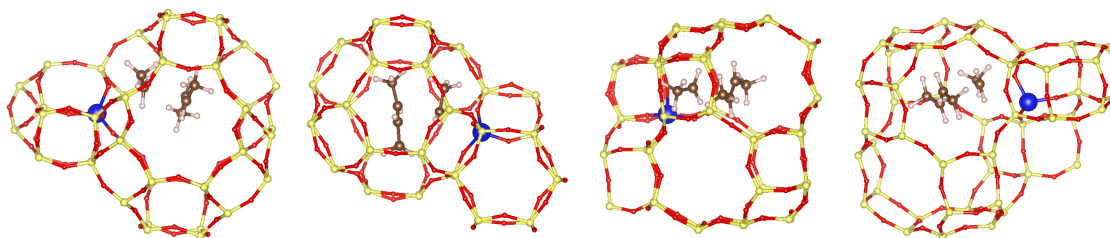


**Fig. S7** Transition structure for the formation of 3-methyl-2-pentene via SES shown from different angles to visualize the orientation of the hydrocarbon chain inside the pore of the zeolite. Color code: oxygen (red), silicon (yellow), aluminum (blue), carbon (brownish), hydrogen (whitish).

